

FACTORS CONTROLLING CRITICAL SHEARS FOR DEPOSITION AND EROSION OF INDIVIDUAL GRAINS

ROBERT F.L. SELF¹, ARTHUR R.M. NOWELL² and PETER A. JUMARS²

¹Friday Harbor Marine Laboratories, NJ-22, University of Washington, 620 University Road, Friday Harbor, Washington 98250 (U.S.A.)

²School of Oceanography WB-10, University of Washington, Seattle, Washington 98195 (U.S.A.)

(Received August 9, 1988; accepted October 18, 1988)

Abstract

Self, R.F.L., Nowell, A.R.M. and Jumars, P.A., 1989. Factors controlling critical shears for deposition and erosion of individual grains. *Mar. Geol.*, 86: 181-199.

We have quantified critical deposition and erosion shear stresses for individual, fine (24-141 μm), natural quartz particles in a flow chamber with radial parallel flow. In seawater (30‰, 10-15°C), critical erosion shear stresses, as expected, are slightly larger than estimates from previous studies which strove for cohesionless conditions, while critical deposition shear stresses are three orders of magnitude larger than predicted by Hjølstrom (1935) and equal to the stress on a particle settling at Stokes' terminal fall velocity. Manipulative experiments indicate that critical deposition shear stress of medium to coarse silt is little affected by physical-chemical adhesion, bed roughness or microbial adhesion, while critical erosion shear stress is at least doubled by microbial adhesion or bed roughness. Critical stresses for individual grains of comparable size are normally distributed, supporting the concept of well-behaved thresholds for both erosion and deposition. Because the thresholds do not differ greatly in magnitude for particles of a given size, organism-produced and -maintained features (e.g., pits and tubes) can be important in shifting local conditions from erosive to depositional and vice versa.

Introduction

It is not overly difficult to build a device that is suitable for making estimates of critical erosion velocity. Grains stay on the bed as increasing shear (generally produced by increasing flume discharge) is applied, until erosion occurs. In the typical flume experiment, however, it is difficult to establish an objective criterion of initial motion. The first grains to move are those that are in unstable positions, presumably constituting one extreme tail of the distribution of critical erosion stresses. This problem leads to ambiguity and a decided lack of consensus about the definition and measurement of threshold shears for erosion (Lavelle and Mofjeld, 1987). One pre-

sumably would prefer to know the mean stress needed to move grains of a given size (and its variance), but there is no obvious way of estimating this parameter in the typical flume layout. The problem is minimized by laying the bed under a flow regime nearly capable of moving the grains, thus reducing the number that land in unstable configurations (Mantz, 1977a), but the departure of the measured critical shears for erosion (τ_c) from the mean for that grain size or range of grain sizes remains unknown.

The problem of estimating critical shears for deposition (τ_d) is no less important. Deposition is crucial not only to geologists, for the obvious reason that most of the sedimentary record is depositional, but also to geochemists

interested in chemically less permanent deposits (Westrich and Berner, 1984) and to biologists concerned with settlement of larvae on to the bed (Butman, 1987) and with feeding (e.g., Miller et al., 1984). The problem of finding a stable mean has been even more difficult here, because during the disappearance of material from suspension under slowing velocity the first particles to deposit are the largest (e.g., aggregates), most dense or those which by chance are closest to the bottom. Furthermore, even to obtain these estimates requires a device inherently more complex than that for critical erosion measurements, since a uniform suspension must be introduced.

Past field and laboratory studies with silts sought to measure threshold stresses for incipient erosion and deposition of a bulk mixture of particle sizes as opposed to the threshold stresses for incipient motion or deposition of individual grains. There are a number of compelling reasons for examining individual particles in an apparatus which emulates the viscous boundary layer. Modeling of sediment motion (e.g., Graf, 1971, p.85; Partheniades, 1977, fig.4; Middleton and Southard, 1984, pp.167; Wiberg and Smith, 1985, fig.4) begins with the depiction of force balances on individual particles. Modeling deposition rates of silts (e.g., McCave and Swift, 1976) requires precise estimates of the mean and variance of τ_d to calculate $P=1-(\tau_b/\tau_d)$, the "overall probability of a particle sticking to the bed", (where τ_b equals the boundary shear stress) as first proposed by Einstein and Krone (1962) for clays.

Numerous variables affect τ_d and τ_c for fine sediments. Many are difficult or impossible to control or monitor under bulk flow conditions. Even if they are well sorted, bulk sediments can range in particle size by ten times or more. The estimated variance from bulk measurements thus confounds variability among grain sizes with reproducibility for a single grain. The bed shear stresses within the boundary layers of straight and annular flumes are inherently variable, spatially and temporally. The boundary layer exerts control on the rates

of deposition and erosion in its lowermost, laminar portion by acting as a sediment trap (McCave and Swift, 1976) and modulating shear-controlled coagulation and disaggregation (Hunt, 1986) of fine sediments. Salinity, temperature and dissolved organic concentration in addition to particle surface characteristics, volumetric concentration, proportion of clay-sized particles and bed roughness have all been implicated as elements influencing estimates of τ_d and τ_c . The relative importance of each variable can be evaluated only by iteration between theory and manipulative experiment.

We estimate τ_d and τ_c for individual particles in the medium silt to fine sand size range within a radial flow chamber and compare our results with the critical deposition predictions of Hjulstrom (1935) and plane bed critical erosion estimates of Mantz (1977a) and White (1970). The unique characteristics of the radial flow cell (Moller, 1963) allow us to determine the boundary shear stress at which individual particles of known size and shape deposit or erode and thus to generate frequency distributions of critical shear stress for each behavior. We further compare and contrast the effects of electrolyte concentration, bed roughness and microbial adhesion on τ_d and τ_c of 20–30 μm grains. The magnitudes of the fluid and particle variables controlling physical-chemical and organic adhesion, in addition to bed roughness, were manipulated and their effects assessed.

Background

Critical erosion and deposition plots are so widely used in introductory geology and oceanography texts that the trail back to the original data is inordinately tangled. Summary discussions of the mode of sediment transport as a function of grain diameter and flow velocity often reproduce the classic Hjulstrom (1935) plot (e.g., Raudkivi, 1976, p.40; Ritter, 1978, p.221; Reineck and Singh, 1980, p.9; Matthews, 1984, p.41) or a modified version of the Hjulstrom diagram (Allen, 1965, p.109;

Postma, 1967, p.158; Kennett, 1982, p.517) attributed to Sundborg (1956, 1967). Hjultstrom (1935) adopted the limiting deposition velocity results of Schaffernak (1922). Schaffernak's observations were restricted, however, to particles larger than 5 mm. Thus, the limiting deposition velocities for particle sizes less than 5 mm remain unsubstantiated by measurements (as carefully pointed out by Hjultstrom and correctly indicated by a dashed line in Ritter, 1978).

Sundborg (1956) made no measurements of limiting deposition velocity. He accepted Schaffernak's (1922) conclusions for grains larger than 5 mm and Menard's (1949, 1950) flume observations for grains ranging from 0.06 to 0.7 mm that the critical deposition velocity is two-thirds of the critical erosion velocity (Sundborg, 1956, fig. 23).

Menard's (1950) curves for deposition (and erosion) are based on mean velocities calculated from flume discharge and are limited "only to currents less than one meter deep". His conclusion that deposition velocity is two thirds of erosion velocity may be valid since all measurements were made under the same conditions (erosion from and deposition to a rippled bed) and are thus internally consistent. Calculations of τ_d for silts and sands from Menard's data, however, require assumptions of dubious validity; e.g., Sundborg (1956, p.185) assumes for Menard's data "that the mean velocity is 85% of the surface velocity, and that the normal depth for the [erosional] experiments was 4 cm". Menard (1949) reports flume dimensions, water discharge volumes and times, and flow depths for his erosion and deposition velocity measurements. Our re-computed average velocities from his specified discharge rates and cross-sectional area are approximately ten times greater than reported by Menard (1950). It is more likely that Manning's equation (discussed on p.19 of Menard, 1949) was used to compute the critical deposition velocities, but unfortunately the values that Menard used for Manning's friction factor are not given. Estimation of boundary shear stress from Menard's mean velocity

and flow depth data is further complicated by ripples (ripple height not specified) on the sediment surface during deposition. Thus, the skin friction contribution to deposition cannot be separated from that due to form drag produced by the ripples. In short, we can find no objective means of specifying τ_d from the data provided by Menard (1949, 1950).

Only incidental reports of τ_d for silts can be found since Menard's work. Heezen and Hollister (1964), citing Rubey's (1933) measurements of settling velocity versus particle size for galena ($\rho_s = 7.5 \text{ g cm}^{-3}$), suggest that a minimum velocity for transport of silts should be their settling velocity. Gardner and Southard (1975) suggest that initial deposition of oceanic sediments occurs at 0.046 N m^{-2} . Mantz (1980) reports deposition shear stresses for particle size distributions with median diameters of $18 \mu\text{m}$ (range 6–60 μm) and $42 \mu\text{m}$ (range 10–80 μm) of 0.033 N m^{-2} and 0.063 N m^{-2} , respectively.

Several past studies have sought to understand the relationship between τ_e and grain diameter for silts and sands. From observations of the behavior of a silt of $10 \mu\text{m}$ median diameter, Rees (1966) estimated its threshold stress in terms of Shields' dimensionless variables. The intent of the work of White (1970) and Mantz (1977a) was to extend the Shields curve and thereby test the predictions of Bagnold (1956) against those of Shields (1936) concerning the theoretical maximum value of the Shields dimensionless incipient transport stress. Mantz (1977a) and White (1970) sought to minimize the effects of physical-chemical interactions between particles by using tapwater or "softened" tapwater.

Experimental methods

The particles

We obtained quartz reference materials (BCR No. 69, November 1979, from Duke Scientific Corporation, Palo Alto, California) characterized by hydrofluoric acid dissolution, gravitational sedimentation (pipette method)

and pycnometric density measurements. The material was found to be 99.7% silica with a mean Stokes diameter of 38 μm . The mean density of grains (the method corrected for packing) was $2645 \pm 4.8 \text{ kg m}^{-3}$. Particle shape and roundness (cf. Pettijohn, 1975) were determined for individual particles during the erosion-deposition experiments with a $400\times$ magnification stereomicroscope.

The radial flow cell

A radial flow cell (Queue Systems, Parkersburg, West Virginia) designed for measurement of microbial adhesion to surfaces in a precisely defined shear flow (Fowler and McKay, 1980) was used to quantify critical deposition and erosion boundary shear stresses

of individual silt-sized quartz particles ranging from 23 to 141 μm . A cross section through the center of the chamber (Fig.1) illustrates its operation. Liquid enters the radially symmetric chamber axially at a given constant discharge rate (velocity \times cross-sectional area). As the flow chamber cross-sectional area increases with increasing radius, fluid velocity and hence shear stress at the walls decreases radially by ten times across the visible portion of the disk. Sediment particles entering the chamber initially follow the fluid streamlines. Under the influence of gravity and decreasing boundary shear stress they deposit onto the smooth (the sizes of surface deformities are below the resolution of the $400\times$ stereomicroscope) stainless steel surface at varying distances from its center.

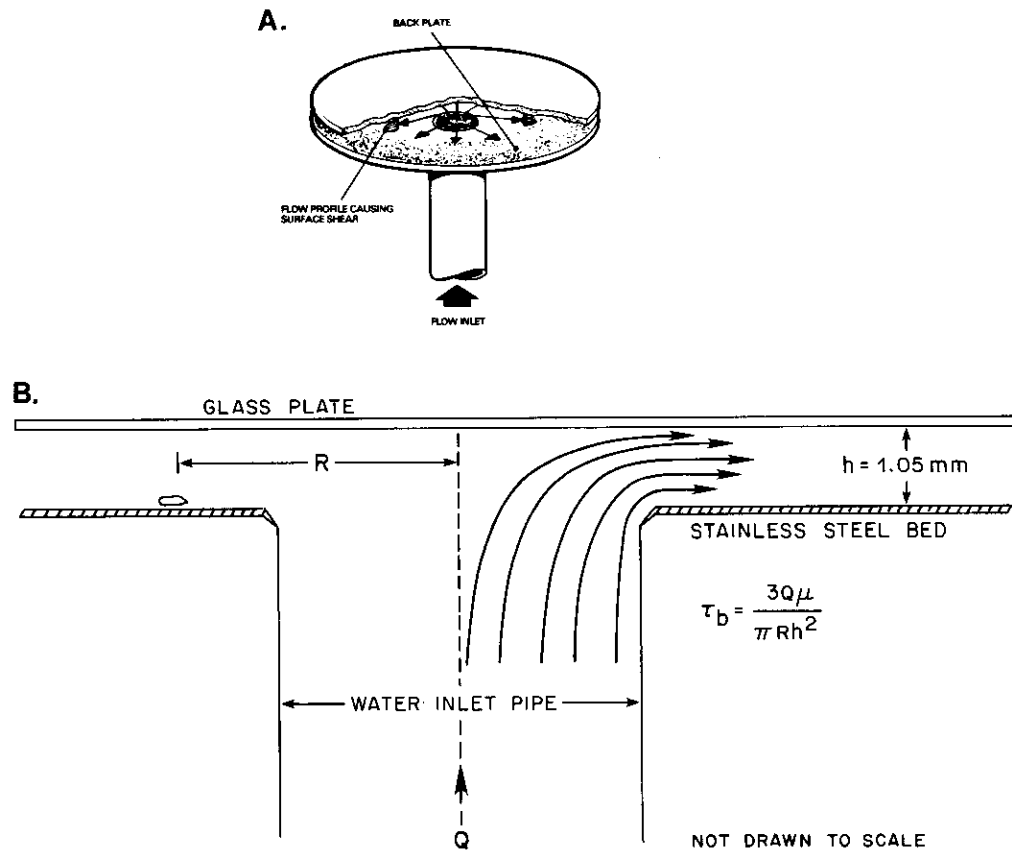


Fig.1. A. Sketch of the radial flow-cell chamber developed by Fowler (Fowler and McKay, 1980). B. Cross-section through the center of the radial flow-cell chamber. τ_b = boundary shear stress at radial distance R from the center of the chamber, Q = liquid discharge rate, μ = liquid viscosity, h = separation distance between the glass plate and the stainless steel bed.

The range of boundary shear stresses across the face of the bed varies with the discharge rate and fluid viscosity (Fig.1). The discharge rate in our open, flow-through system was controlled by varying the height of either the end of the discharge hose or the constant head supply tank relative to the fixed vertical position of the flow-cell chamber. The discharge rate was measured by timing the filling of a graduated cylinder. A 2-mm probe located within the flow-cell chamber 55 mm from the center of the entrance continuously monitored the temperature of the liquid. Salinity samples were taken daily. Viscosities were computed according to Millero (1974).

A disperse suspension of quartz particles, occupying a volumetric fraction (ratio of suspension volume to pipe volume) of less than 0.05% and thus minimizing interparticle collisions (Davis and Acrivos, 1985), was injected via syringe and needle into the water stream flowing through a 5-mm (I.D.) tube. The end of the needle and last right angle bend were 36 and 437 mm, respectively, upstream from the entrance to the flow-cell chamber.

The physical dimensions of the flow-cell chamber limit the maximum particle size that can be used and the maximum wall shear stress that can be developed. To minimize disruption of the velocity profile near the wall a ratio of maximum particle size to separation distance between the glass plate and stainless steel bed (h) of 1:7 was maintained. At discharge rates of approximately $2.8 \times 10^{-6} \text{ m}^3 \text{ s}^{-1}$, which correspond to a maximum boundary shear stress of 1 N m^{-2} , an intermittent recirculation cell begins to form at the entrance to the chamber, re-attaching a few millimeters downstream. Our maximum discharge rates were kept below this value. A fuller discussion of the flow characteristics of the radial flow cell can be found in Moller (1963).

Critical deposition shear stress versus particle size

A subsample of the particle mixture (size range 14–141 μm) was mixed with a 0.25% non-

ionic surfactant (Triton X-100™) in filtered saltwater solution in an attempt to minimize particle aggregation from water surface tension. The stainless steel surface was cleaned with a laboratory soap solution to remove accumulated organic film. After assembly of the flow cell, tapwater was circulated at a high discharge rate (50×10^{-6} – $83 \times 10^{-6} \text{ m}^3 \text{ s}^{-1}$) in order to remove air bubbles from the system. Filtered seawater from the head tank was then routed to the flow-cell chamber, displacing the tapwater (indicated by water temperature change). The discharge rate (and thus the range of boundary shear stress in the chamber) was then set to a level that pretests suggested was sufficient to transport the largest particles (141 μm) up the entrance pipe, but that was small enough to allow the smallest visible particles (20–30 μm) to deposit somewhere on the stainless steel disk. During deposition, three replicate discharge rate measurements were taken (coefficient of variation $\pm 6\%$), water temperature was recorded and a water sample was taken for salinity determination. After all the particles were deposited the discharge rate was decreased by 80–90%, at which time individual particle lengths and widths and distances from the center of the chamber were recorded.

Radial distances were measured to the nearest 0.2 mm by radial traverses of a stereomicroscope with calibrated eyepiece grid along three randomly selected (from four) guidelines drawn on the surface of the top glass plate of the cell chamber. A calibrated eyepiece reticle was used to measure the major and minor axes of the particles (maximum length and maximum width orthogonal to the length axis). The limit of resolution of the stereomicroscope (20–30 μm) prohibited data collection on the smallest particles present. Equivalent diameters of the particles were computed assuming that the unmeasurable vertical dimension equaled the lesser of the two measured dimensions; the equivalent spherical diameter then, is proportional to the cube root of the computed particle volume.

Critical erosion shear stress versus particle size

In another set of measurements particles were deposited in a shear flow as described above for subsequent evaluation of critical erosion shear stress of individual particles. Particles deposited in a shear flow (as opposed to still water) are more likely to be in erosion-resistant configurations on the bed (Mantz, 1977a). After all the particles had been deposited, the discharge rate was decreased by 80–90% and up to ten particles in one field of view at a randomly selected radial position were monitored simultaneously with the stereomicroscope. Particle size measurements were recorded and a sketch of their positions drawn with respect to each other and the fluid velocity vector. The boundary shear stress was then increased in increments of 0.05 N m^{-2} every minute until one or more of the monitored particles moved at least a particle diameter downstream (upon initial motion, 90% of the eroded particles left the field of view of the stereomicroscope); then, the temperature was recorded, a water sample for salinity determination taken, and three replicate measurements of the discharge rate made. The boundary shear stress was increased stepwise in this manner until all the monitored particles had been eroded or the maximum boundary shear stress of approximately 1 N m^{-2} at the flow cell entrance had been reached. Of the 116 particles monitored, 96 or 83% eroded before the maximum boundary shear stress was reached. For any one of the fourteen size categories, more than two thirds of the particles observed were eroded. The critical erosion shear stress was computed only for those particles that were actually eroded.

Manipulative experiments

Critical deposition and erosion shear stresses were measured for individual 20–30- μm particles in four liquid–bed–particle coating combinations or treatments. In addition to filtered seawater, pure water from the storage

tank of a reverse-osmosis (RO) water purifier (Technic Control Systems, Seattle, Washington) allowed evaluation of erosion and deposition in conditions of minimal physicochemical adhesion. As another treatment, the smooth stainless steel surface of the flow cell was roughened by gluing down particles with rubber cement. This procedure allowed evaluation of the effects of a fixed, rough bed. Microbes were cultured on the surface of particles to evaluate biologically induced adhesion effects. The four treatment combinations evaluated were: (1) RO water, smooth bed, clean particles; (2) seawater, smooth bed, clean particles; (3) seawater, rough bed, clean particles; and (4) seawater, smooth bed, microbe-coated particles.

Twelve variables were monitored in these experiments. Variables related to the fluid included salinity, temperature, discharge rate, dissolved organic nitrogen and carbon, and bacterial concentration. Variables related to the bed were roughness, critical contact angle and contact angle with the treatment liquid (indicative of freedom of the bed material from adsorbed organic coatings). Submergence time in the treatment liquid, surface microbial abundances and proportion with greater than 50% coverage of organic matter or microbes were monitored for the particles.

The particles were altered further for the manipulative experiments. Those less than 20 μm were removed by sieving with a Nitex™ screen to prevent secondary cohesive effects (i.e., bed–particle–particle rather than bed–particle cohesion) between 20–30 μm particles and < 20 μm particles. The remaining particles were cleaned by submersion in hot, concentrated sulfuric acid for 30 min, then repeatedly rinsed with RO water. After drying at 60°C overnight the particles were stored in a desiccator.

To prepare microbe-coated particles, the > 20 μm fraction described above was submerged in a saltwater culture medium with 0.01% peptone and 0.001% yeast extract and then kept at room temperature and aerated for 16 days, at which time the particle surfaces

exhibited natural levels of microbial coverage. Deposition, then erosion runs with these particles took another 17 days, over which time particle microbial concentration increased by a factor of 19.

In addition to salinities, the relative concentrations of macromolecules that could adsorb to the cleaned particle surfaces and thus could influence the particles' surface properties, was approximated by measurements of dissolved organic carbon (DOC) and nitrogen (total nitrogen minus nitrate, nitrite, ammonia and particulate nitrogen concentrations). Our epifluorescence microbial enumeration techniques of liquids and particles, with the acridine orange stain, employed standard procedures and controls (Parsons et al., 1984).

Bed and particle surface tensions determine the sign and magnitude of the surface interaction. The critical surface tension (a comparative estimate of surface energy) of the stainless steel plate (before submergence in treatment water) was estimated using the techniques of Bernett and Zisman (1968). "High-energy" solid surfaces, such as glass and metals, "pull" liquids of lower surface tension out in all directions at the liquid-gas-solid interface. The liquid drop spreads over the surface; the acute angle formed at the intersection of liquid and solid is called the contact angle. The critical surface tension of a solid is estimated by extrapolation of a Zisman plot. To generate a Zisman plot the liquids we used were diiodomethane, 1-bromonaphthalene, propylene carbonate and dicyclohexane with surface tensions of 51.0, 44.6, 41.6, and 32.8 mN m⁻¹, respectively. The 20–30 μm particle size precluded measurements of the surface properties of individual grains. We thus assumed surface tensions of 26–42 mN m⁻¹ as reported by Bernett and Zisman (1969) for such quartz surfaces.

The stainless steel plate was prepared for a run (except fixed rough bed) by first cleaning with a commercially available oven degreaser (Mr. Muscle™, Drackett Products Company). Following rinsing with treatment water and swab-drying with tissue paper, up to three

drops of treatment water were placed at various locations on the plate and the contact angle measured with a Questar™ long-range microscope with eyepiece reticule calibrated for measurement of angles (goniometer).

The sequence of events in the RO water, smooth bed, clean particles; seawater, smooth bed, clean particles; and seawater, smooth bed, microbe-coated particles treatment runs followed closely those described for the deposition-erosion versus particle-size runs. The seawater, rough-bed, clean-particles procedures were different from the other treatments because of the difficulties of removing the colloidal residue left by the degreaser without dislodging the glued-down particles and because of the difficulties in differentiating the transparent, glued-down particles, the source of bed roughness, from the also transparent, depositing, 20–30 μm particles. The former difficulty was mitigated by not cleaning the bed after each run. Instead, only a portion of the bed was roughened by making two equally spaced and radially symmetric 1-cm wide swaths of glued-down particles. By depositing or eroding particles from the smooth portion of the bed, the effect of not cleaning the bed over time (16 days) could be quantified if necessary by comparison with past smooth-bed runs in which the plate had been cleaned. The second difficulty was alleviated by fixing the position of the stereomicroscope for each run in order to view the rough bed at a randomly selected radial distance from the center; we then counted the number of 20–30 μm particles depositing at the observed radial distance. The mean boundary shear stress could then be calculated from particle frequency versus radial distance.

The seawater, rough-bed, clean-particles erosion procedure began by viewing, on alternating runs, the smooth- or rough-bed portions of the plate at a radial distance where 20–30-μm incoming particles were likely to deposit. The difficulty of distinguishing erodible from fixed particles forced us to monitor no more than two particles per run. The shear stress was

then increased, as previously described, until the monitored particles eroded or the maximum shear stress was reached. A WildTM compound microscope with an eyepiece micrometer calibrated in 13.7- μm intervals and the fine focus calibrated in 1- μm intervals was used to transect the rough-bed portions of the plate.

Statistical procedures

The ordinate of the Hjølstrom (1935) plot is velocity 1 m above the bed. To convert it to units of boundary shear stress (N m^{-2}) the equation for the logarithmic velocity profile, $U(z) = (u_* / \kappa) \ln(z/z_0)$, was solved iteratively for $u_* = (\tau_b / \rho)^{1/2}$ where τ_b = boundary shear stress and ρ = the liquid density. The Von Karman constant, κ , equals 0.41. In our experiments, the boundary Reynolds number, $u_* k_s / \nu$, where k_s equals particle size and ν , the kinematic viscosity, was always less than 3. Thus, the roughness length, z_0 , is estimated by $\nu / 9u_*$ (Smith, 1977).

The replicate critical shear stress measurements for each particle size were combined and separate frequency distributions generated for τ_c and τ_d . We first computed a mean critical shear stress ($\bar{\tau}$) from the replicate measurements for each particle size. The residuals ($\tau - \bar{\tau}$) for any one particle size class were determined and then combined (pooling justified as the standardized distributions all have a mean of zero) with residuals for the other particle sizes.

If the assumptions of parametric statistical models were valid, they were used in data analysis; otherwise, nonparametric correlation and linear regression analysis (Tate and Clelland, 1957; Hollander and Wolfe, 1973) were substituted. One-way analysis of variance (ANOVA) followed by inspection of the ANOVA model residuals for correlation with the potential covariables (Box et al., 1978), and tests of the independence of frequency data (4×2 contingency table; Sokal and Rohlf, 1969) were applied to the results of the manipulative experiments.

Results and discussion

We recognize that boundary-layer structure and dynamics in the flow cell are not identical to those found in nature. Clearly the flow cell is unlikely to reproduce bursting or flow-parallel wall streaks of a natural scale. Because there is no theory to allow us to do otherwise, however, we quote mean values of flow parameters calculated for the flow cell and explicitly assume that the same mean values in nature will produce the same effects in terms of erosion or deposition. We suggest that making this provisional assumption is less dangerous than continuing to discuss deposition without data. Furthermore, extant models of sediment transport deal with mean quantities. If models become available that relate erosion and deposition to the full frequency distributions of fluid forces in the field, then our explicit assumption can be modified appropriately.

Critical deposition shear stress versus particle size

The radial distance at which a particle comes to rest, i.e., deposits, is in part determined by its position in the stream when it enters the flow-cell chamber. All else being equal, a particle entering the flow-cell chamber between the bed and the middle height of the chamber would initially touch the bed (but not necessarily cease moving) at a smaller radial distance (higher boundary shear stress) than a particle that entered between the upper glass plate and mid-height (Fig.1). We were unable to control the position of a particle entering the flow-cell chamber. This uncontrolled variable could lead to overestimates of the magnitude of the τ_d and certainly does increase the variability of an estimate. To counteract this design problem, we modeled the trajectory of a particle by: starting it in contact with the upper plate at the flow cell entrance (i.e., $R=0$ in Fig.1), instantaneously accelerating it to the velocity of the liquid at that radial and vertical position, and then allowing the particle to settle vertically at its expected Stokes settling

velocity and move radially with the local (hyperbolically varying) horizontal velocity. Using the modeled final resting radial distance of the particle as a cutoff, we calculated our estimates of τ_d only from particles found at greater radial distances. Thus, each assayed particle should have first reached the bed upstream of the point at which it came to rest. This method gives conservative estimates of τ_d , which are closer to Hjulstrom's (1935) prediction than if our cutoff were not used.

Our measurements of τ_d (Fig.2) are about three orders of magnitude greater than Hjulstrom's prediction (as guessed by McCave and Swift (1976) in their parenthetical introductory remarks), which was based on an extrapolation of a single data point for 5-mm gravel. Critical deposition boundary shear stresses for individual grains are likely to be normally distributed, as indicated by the frequency distribution of our measurements (Fig.3A). The observed distribution does not differ significantly from a normal one when examined with the Kolmogorov-Smirnov one-sample test ($P=0.8$).

The equations which best predict the slope of

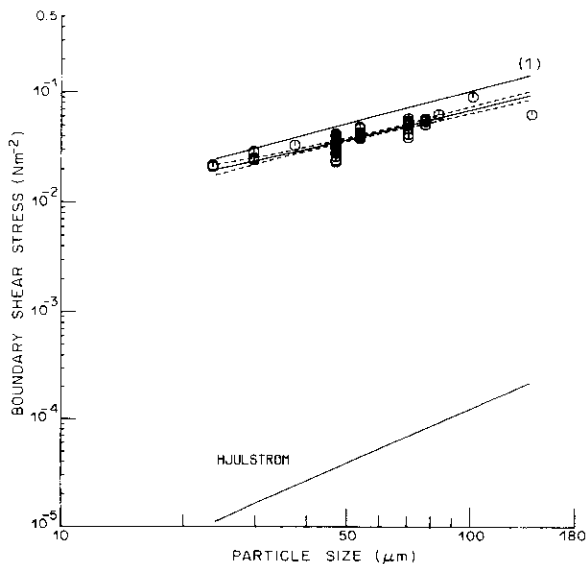


Fig.2. Critical deposition boundary shear stress versus particle size for Hjulstrom's (1935) prediction, this study (○, nonparametric linear regression with 95% confidence limits), and predicted based on Stokes' settling velocity (I).

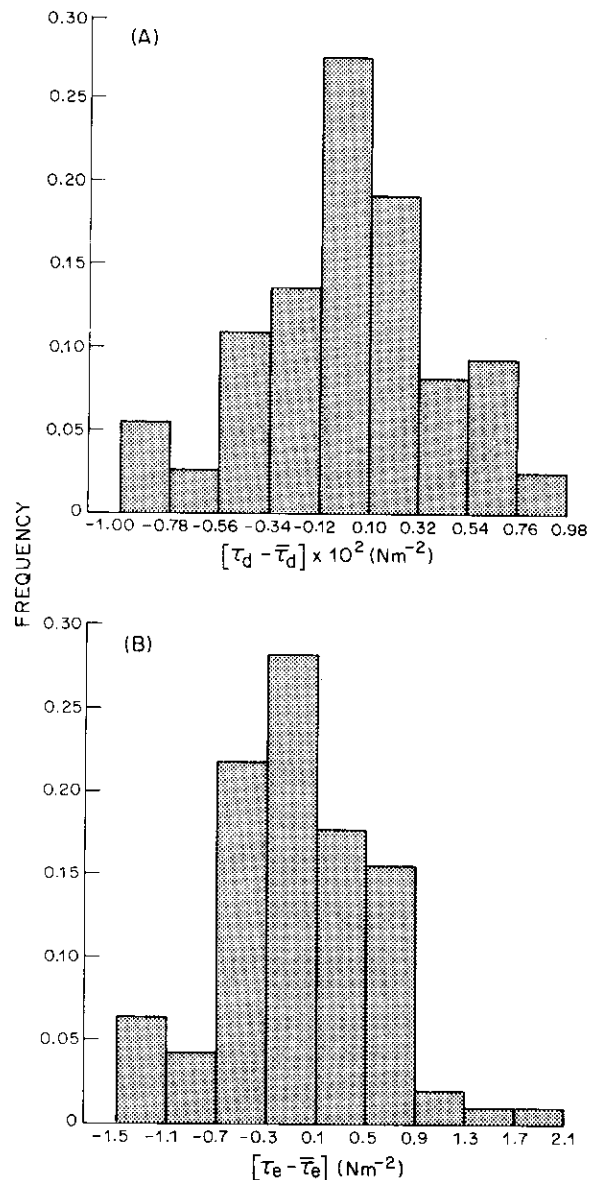


Fig.3. Frequency distributions of critical deposition (A) and erosion (B) boundary shear stresses for single grains.

our regression line are, however, formulations based on Stokes' law, where the force per unit area on a sphere (τ_s) of diameter d , settling at velocity U , in a fluid of viscosity μ , at a Reynolds number less than one ($Re=0.1-1.0$ in our deposition experiments) is $3\mu U/d$ (Tritton, 1977). If U equals the terminal settling velocity of the particle, then τ_s equals the critical deposition stress of the particle assuming a

sphere falling through a quiescent fluid or, conversely, a sphere suspended by a fluid moving vertically at the terminal fall velocity of the particle. Given that in our flow cell the fluid is moving parallel to the boundary, however, with consequent development of a velocity gradient and shear stress, what then is the relationship between boundary shear stress and critical deposition stress?

The stress we estimate from the flow cell calibration is that which would occur on the bed at the final resting position of the particle in its absence, rather than the total stress acting on the particle per se. Goldman et al. (1967), O'Neill (1968) and Hubbe (1981, pp.124-125) submit that the total force, F_s , on a sphere in contact with a plane bed (neglecting adhesion forces) is equal to $A\tau_b(2.55)$, where A is the surface area of the sphere and τ_b is the shear stress on the boundary without particles. The average force per particle surface area, $\tau_s = F_s/A = 2.55\tau_b$, or equivalently, $\tau_b = 0.39\tau_s$. Thus, the shear stress on the bed in the absence of particles (our measurements) is predicted to be 39% of the total (pressure + shear) stress on the particle per se. Setting τ_s equal to the total stress on a particle settling at its terminal fall velocity we predict τ_b , the boundary shear stress at which natural quartz particles should deposit (Fig.2). The agreement between theory and measurement is surprisingly good. The slope of our best-fit regression line is not significantly different ($P=0.05$) from the slope of the expected relationship. The expected values of τ_d are slightly higher, however, than our measurements. This discrepancy could be due to the shape difference between spheres and natural grains or to flow effects of previously arriving grains in the vicinity of the final resting position of the particle.

Critical erosion shear stress versus particle size

One objective in measuring critical erosion boundary shear stress for incipient motion was to allow measurements from the flow-cell apparatus to be placed in the context of past

studies. Our results for seawater, plotted in Fig.4 along with the best-fit line for the initial transport results of White (1970) and Mantz (1977a), confirm that the flow cell gives comparable critical shear stresses. We take this observation as support of the ability of the flow cell to produce fluid dynamic conditions useful in the study of sediment transport and of our explicit assumption that mean quantities can be equated from the flow cell, through flume studies, to the field. The frequency distribution of our data, combined among particle sizes (Fig.3B), suggests a well-behaved Gaussian distribution ($P=0.4$, Kolmogorov-Smirnov test), allowing the idea of a threshold shear to be defined unambiguously.

The criteria employed by Mantz (1977a) and White (1970) to determine critical stresses for erosion are subjective (and thus potentially inaccurate) but nevertheless precise; 95% confidence intervals for White's (1970) data are estimated from his standard deviations about mean Shields dimensionless threshold stresses

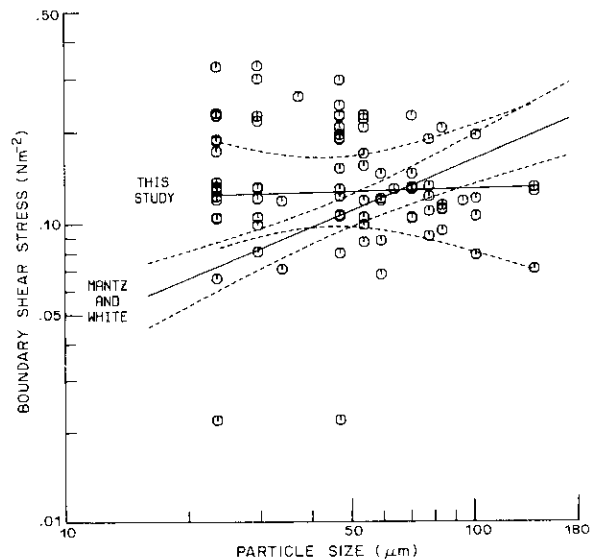


Fig.4. Critical erosion boundary shear stress for initial motion versus particle size. Circles are our measurements for individual particles. Continuous lines are results of parametric least-squares regressions for our measurements and the un-plotted measurements of Mantz (1977a) and White (1970). Dashed lines are 95% confidence limits for the estimated mean shear stress.

to be about $\pm 11\%$ of their means. Given the small variances of their data, a highly significant linear regression of \log_{10} -transformed values ($P < 0.001$) with very tight 95% confidence intervals about the regression line results. In comparison, the variance of our data for τ_c for individual particles is large and tends to increase with decreasing particle size. Nonparametric correlation analysis of our data suggests a weak negative correlation between τ_c and particle size (Kendalls coefficient = -0.12 , $P = 0.077$). The slightly positive linear regression slope for our data is not significantly different from zero, and our τ_c predictions at the 0.05 alpha level are not significantly different from those of Mantz and White for the range of particle sizes tested. Given the great difference in electrolyte concentration between the eroding liquids (conductivity of water for our measurements about $32,000 \mu\text{mhos cm}^{-1}$ versus $700 \mu\text{mhos cm}^{-1}$ for Mantz (1977a); White (1970) also used tapwater) the mild disparity of these results is not unexpected.

Probably the most widely accepted (although untested) explanation for the disparity in the trends of the saltwater versus freshwater data sets would invoke the paradigm of interacting surface energies (e.g., Mantz, 1977b) popularly known as the DLVO theory after its developers Derjaguin and Landau (1941) and Verwey and Overbeek (1948) (see Van Olphen, 1966; Overbeek, 1982; Schowalter, 1984; Loeb, 1985, for recent updates). Briefly, the theory predicts that at high electrolyte concentrations and small intersurface separation distances, the London–Van der Waals attractive interaction energy will be greater than the repulsive (assuming particles and plate are negatively charged; Loeb and Neihof (1975), Hunter and Liss (1979)) interaction energy of the electric double layer, and fine particles will tend to stick to each other, or, in the case of the flow cell, to the stainless steel plate (see Bowen (1978) and Bowen and Epstein (1979) for a discussion of the sphere–plate interaction). Thus, the finest particle sizes in saltwater are predicted to be more difficult to erode than the

same particles in freshwater. The gross effects of electrolyte concentration can be predicted using DLVO theory. In most field situations, however, electrolyte concentration is homogeneous, and there are other mechanisms of particle resistance to erosion. Our manipulative experiments explicitly examined bed roughness and microbial adhesion, in addition to electrolyte concentration, and sought to compare their effects on critical erosion and deposition shear stress of the finest particle size (most susceptible to the relatively small adhesion forces) that we could observe reliably. The spirit of these manipulative experiments was to detect order-of-magnitude differences.

Manipulative experiments

The potential nuisance variables over which we were not able to exert total control (and thus which could have causally covaried with boundary shear stress) are presented in Table 1 with the salinity and particle bacterial abundances. Briefly, water bacterial concentration and dissolved organic nitrogen (DON) in RO water were less than in natural seawater. Surprisingly, DOC was approximately equal in the two water types. The contact angle and particle submergence time were independent of water type; as expected, natural seawater temperatures (experiments performed between November 1985 and May 1986) tended to be a few degrees lower than in the RO water, stored at room temperature. Figure 5 gives one an impression of the characteristic roughness of the bed and the frequency of pockets large enough to hide a $25\text{-}\mu\text{m}$ particle.

Physical–chemical attraction or repulsion between the silica particles and the metal bed are in part determined by the surface tension or energy of the metal bed (Fig. 6). Our estimate of critical surface tension of the metal surface compares well with literature values for quartz or glass ($26\text{--}42 \text{ mN m}^{-1}$; Bernett and Zisman, 1969), and metals ($38\text{--}45 \text{ mN m}^{-1}$; Bernett and Zisman, 1968); bear in mind that the surface energy will decrease, after submergence in

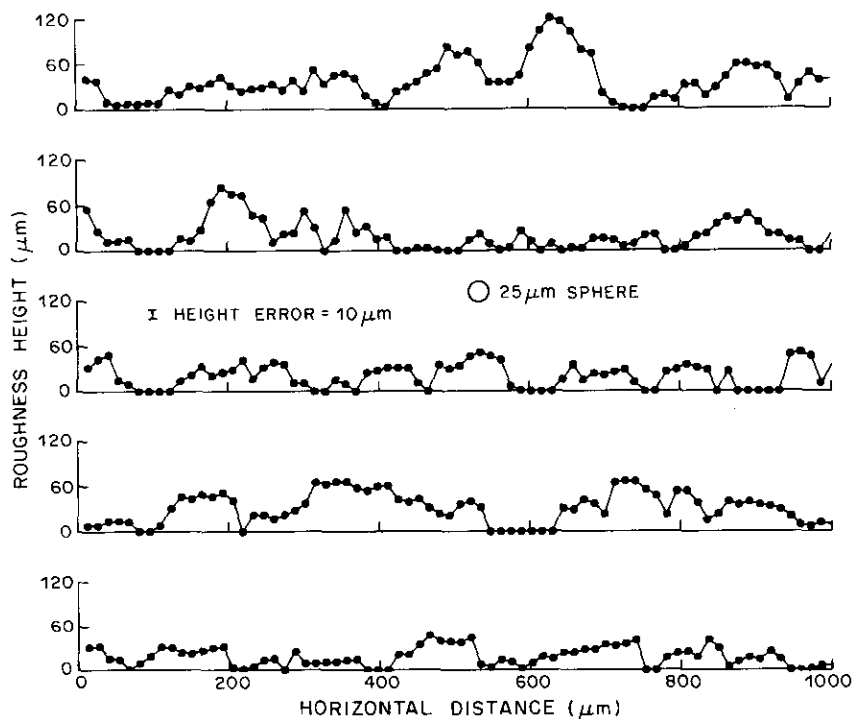
TABLE 1

Means and twice the standard deviations of liquid, bed and particle variables

	Deposition		Erosion	
	RO* water Mean \pm 2SD	Seawater Mean \pm 2SD	RO water Mean \pm 2SD	Seawater Mean \pm 2SD
Salinity (‰)	0.04 \pm 0.02	30.80 \pm 0.40	0.03 \pm 0.02	30.70 \pm 0.60
Particle bacterial concentration ($\times 10^4$ ind. mm^{-2})		6 \pm 4		23 \pm 19
Water bacterial concentration ($\times 10^4$ ml^{-1})	0.2 \pm 0.2	8.0 \pm 14.0	0.4 \pm 0.6	6.9 \pm 12.0
Contact angle (degrees)	17 \pm 5	12 \pm 8	13 \pm 3	11 \pm 6
Particle submergence time (h)	3 \pm 6	3 \pm 7	2 \pm 4	3 \pm 5
Dissolved organic nitrogen (mg l^{-1})	0.07 \pm 0.08	0.29 \pm 0.29	0.05 \pm 0.002	0.31 \pm 0.34
Dissolved organic carbon (mg l^{-1})	1.81 \pm 0.82	2.19 \pm 1.10	1.82 \pm 0.28	2.09 \pm 1.03
Water temperature ($^{\circ}\text{C}$)	15.7 \pm 1.3	12.2 \pm 4.0	16.4 \pm 2.3	10.6 \pm 2.1

*Reverse-osmosis processed tapwater.

ind. — individuals.

Fig.5. Results of microscope transects of the surface roughened by gluing 20–141 μm natural quartz particles to the stainless steel bed of the radial flow cell. Minimum precision of height measurements is $\pm 10 \mu\text{m}$.

water, to about 20 mN m^{-1} (equivalent units are Jm^{-2}) as more water molecules adsorb to the surface (Shafrin and Zisman, 1967). Thus, our estimate of 34 mN m^{-1} represents the starting condition of the clean metal surface.

The critical deposition boundary shear

stress of individual, fine silt particles is not significantly affected by electrolyte concentration, adhesiveness of the particle coating or the roughness of a bed, if the latter is constructed of fine silt particles (Table 2, Fig.7). The slightly larger mean shear stress

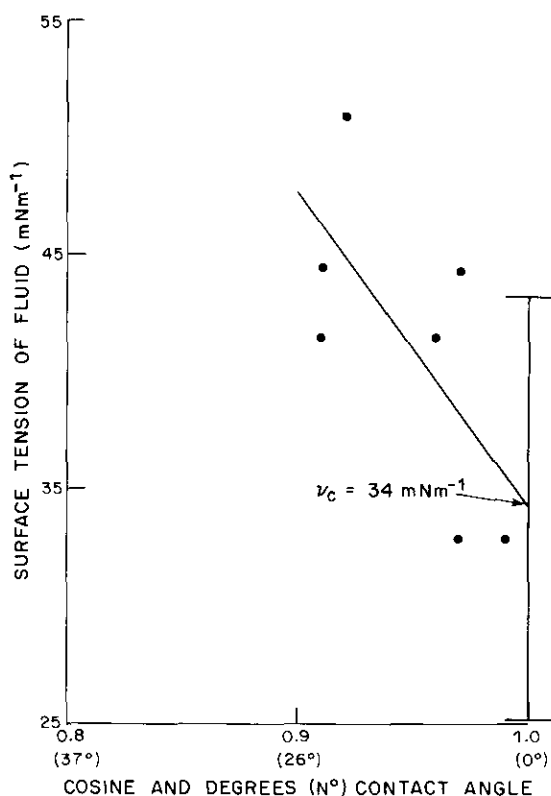


Fig.6. Estimate of critical surface tension $\pm 95\%$ confidence interval for the exposed stainless steel surface of the radial flow cell before submersion.

and significantly lower proportion ($P=0.05$, after accounting for multiple testing, of the equality of two percentages; Sokal and Rohlf, 1969, p.607) of observed particles which passed our conservative criteria suggest that bed

roughness is probably the most important determinant of τ_d extrinsic of particle characteristics (e.g., settling velocity). The larger proportion of particles that passed our criteria in the other three treatments indicate that relatively more particles continued to move toward a region of lower shear stress (greater radial displacement from the inlet) after initial contact with the smooth bed. Neither physicochemical nor biological adhesion, acting on very small time scales of a particle collision with the bed, appear to extract as much particle momentum as contact with the fixed, rough bed.

ANOVA (Table 3) clearly indicates that some of the treatment conditions changed τ_c (Fig.8). The results of multiple comparison testing suggest that physicochemical adhesion has little effect on the erosion of 20–30- μm particles, as no significant differences between the mean τ_c of the RO-water, smooth-bed, clean-particles and the seawater, smooth-bed, clean-particles treatments are detectable. Modeling the sphere–plate interaction (equations from Bowen, 1978, pp.14–28) in the two different liquids (Fig.9) also suggests that for a particle size of 25 μm the attractive energy in seawater between the particle and plate is less than 5% of the torque required to just move the particle. The large predicted repulsive energies for the same sized sphere in RO water, 45,000 times greater than the torque required to just

TABLE 2

Results of ANOVA and a nonparametric analysis of critical deposition boundary shear stress (N m^{-2}) for 20–30- μm natural quartz particles under varying conditions of electrolyte concentration (freshwater versus seawater), particle coating (clean versus bacterially coated surface) and bed roughness (smooth versus roughened bed). ns — not significantly different at $P=0.05$

Source of variation	Sum of squares ($\times 100$)	d.f.	Mean square ($\times 100$)	F	P
Between treatments	25.07	3	8.36	0.54	ns
Between runs	230.94	24	9.62	0.62	ns
Within runs	2140.54	137	15.62		
Total	2396.55	161			

Multiple comparison results based on (nonparametric) tests of equality of the proportions of observed particles that deposited at shear stresses lower than would be expected based solely on their settling velocities. Underlined treatments are not significantly different at $P=0.05$.

RO water Seawater Bacteria Rough bed

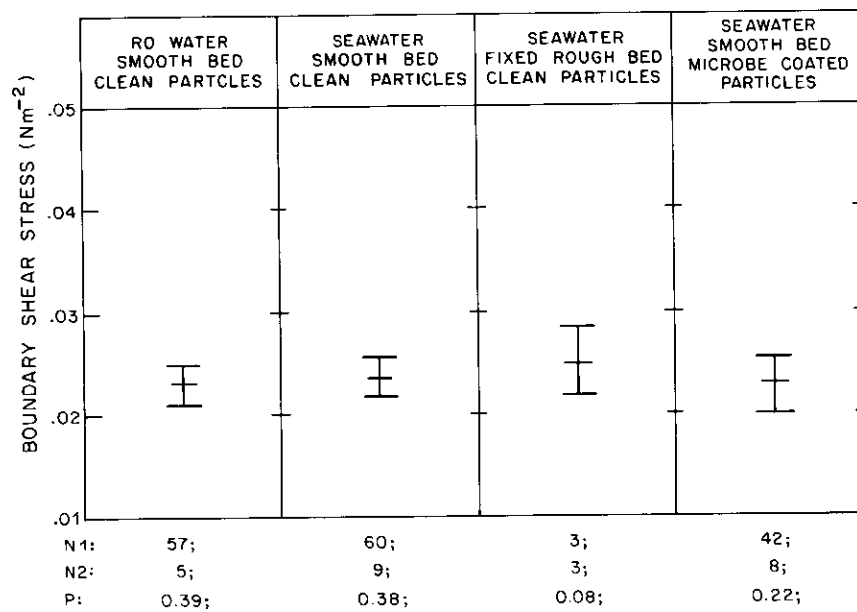


Fig.7. Mean \pm 2SD intervals of critical deposition boundary shear stress for 20–30- μ m natural quartz particles under four treatments that vary liquid electrolyte concentration, bed roughness and particle coating. $N1$ — number of particles; $N2$ — number of treatment replicates; P — proportion of observed particles that deposited at shear stresses lower than would be expected based solely on their settling velocities.

TABLE 3

Results of ANOVA and a nonparametric analysis of critical erosion boundary shear stress ($N m^{-2}$) for 20–30- μ m natural quartz particles under varying conditions of electrolyte concentration (freshwater versus seawater), particle coating (clean versus bacterially coated surface) and bed roughness (smooth versus roughened bed)

Source of variation	Sum of squares ($\times 100$)	<i>d.f.</i>	Mean square ($\times 100$)	<i>F</i>	<i>P</i>
Between treatments	7.50	3	2.50	12.50	<0.001
Between runs	21.30	36	0.59	2.95	0.004
Within runs	5.70	28	0.20		
Total	34.50	64			

Parametric multiple comparison results based on mean τ_c . Underlined treatments are not significantly different at $P=0.05$.

RO water Seawater Rough bed Bacteria

Multiple comparison results based on (nonparametric) tests of equality of the proportions of observed particles that eroded. Underlined treatments are not significantly different at $P=0.12$.

RO water Seawater Rough bed Bacteria

move the sphere, do not substantially affect the particle resistance to movement, since particle inertia and friction with the bed must still be overcome before initial motion occurs. Another line of evidence, the proportion of observed particles which eroded at or below

the maximum shear stress obtainable (Table 3, Fig.8), are also not significantly different between the RO-water and seawater treatments under identical bed-roughness and particle-coating conditions. In both treatments the proportion of observed particles that

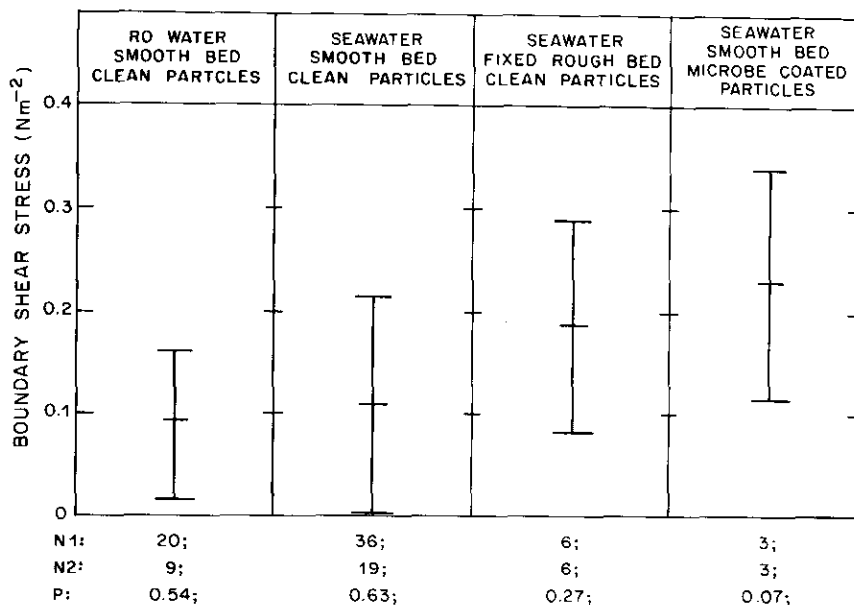


Fig.8. Mean \pm 2SD intervals of critical erosion boundary shear stress for 20–30- μ m natural quartz particles under four treatments that vary liquid electrolyte concentration, bed roughness and particle coating. *N1* — number of particles; *N2* — number of treatment replicates; *P* — proportion of observed particles that eroded.

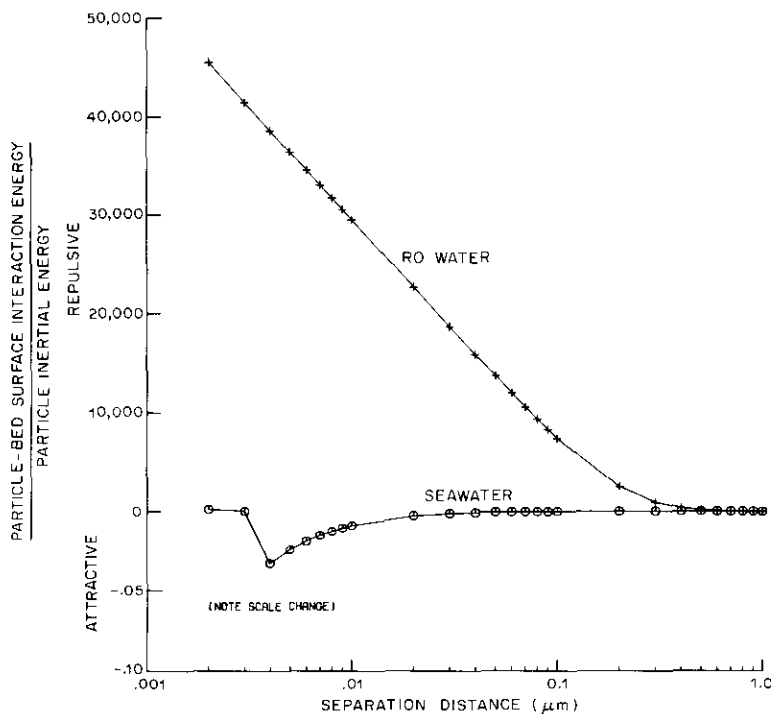


Fig.9. Predicted particle bed surface interaction (scaled to particle inertia) for a 25- μ m diameter quartz sphere versus separation distance between particle and bed surfaces. The ordinate gives the modeled interaction energy (in Joules, equations of Bowen, 1978, pp.14–28) divided by torque required to just move the particle. We calculated critical torque as particle weight in water times particle radius, i.e., force acting parallel to the bed on the particle at one particle diameter from the bed.

eroded is greater than 50%, and thus one can estimate the median τ_c for each of these two treatments; the medians were equal at 0.16 N m^{-2} .

Our experiments separated the effects of bed roughness and microbe coating on τ_c (Fig. 8, Table 3). Either condition at a minimum doubles τ_c . Mean τ_c values for these treatments are gross underestimates, as less than one half of the observed particles moved at or below the maximum boundary shear stress obtainable in our device (1 N m^{-2}). Thus, although we cannot give a median estimate of the boundary shear stress required to set a 20–30- μm particle in motion when within a small pocket or coated with microbes and their associated organic secretions, it is clear that this stress exceeds 1 N m^{-2} , which itself is about an order of magnitude greater than the smooth-bed, clean-particle case.

Evidence of the importance of biological adhesion on critical stress for incipient transport (τ_{cr} , sensu Mantz, 1977a) from bulk measurements is increasing. Parchure and Mehta (1985) and Montague (1986) cite the laboratory experiments of Parchure (1984) in which the τ_{cr} of kaolinite beds was measured with and without microbes. τ_{cr} for the clay beds with microbes was 60% higher than without microbes. Field (Grant et al., 1982) and laboratory (Nowell et al., submitted) experiments with sand-sized grains also indicate that τ_{cr} can be doubled due to the effects of biological adhesion. Thus, the effects of biological adhesion are not restricted to only a small portion of the sediment size spectrum. The reasons for advocating "setting times" (Partheniades, 1984b) and "equilibration" periods (Mehta and Partheniades, 1982) of a few weeks are now clear. Time must be allowed for microbes to grow and proliferate before abiotic sediments can be used in experiments, otherwise an important if not dominant variable influencing sediment movement is missing. The natural follow-up question is whether most microbial communities in the laboratory and nature have comparable adhesive effects.

The design of our manipulative experiment

did not allow us to explore interactions between water type, bed topography and organic "stickiness" of the particles. For example, is the effect of bed roughness and microbial coating, acting in concert, to increase τ_c linearly, or exponentially? In nature, sedimentary particles are lying on non-uniform surfaces and are coated with microbial exudates. We would predict that the interaction effect is nonlinear since the number of contact points and therefore the area of adhesive interaction increases when particles are situated in pits and crevices created by other particles.

We removed the smallest particles ($< 20 \mu\text{m}$) in order to minimize the number of variables. In natural sediments, silt, sand and clay are mixed. The mineralogy and proportion of very small particles ($\leq 2 \mu\text{m}$) are thought to exert control over the magnitude of cohesion (Owen, 1977; Kamphuis and Hall, 1983). The effects of either variable could be determined with manipulative experiments utilizing a radial-flow chamber. For example, silts could be mixed with clays of known mineralogy and quantity, then deposited onto and subsequently eroded from the bed.

Implications

The concept of critical bed stresses for incipient transport (Lavelle and Mofjeld, 1987) and deposition (Partheniades, 1984a) can be misleading because the stresses are usually implicitly associated with the mean or median particle size, when in fact the sizes of the particles depositing or transporting are unknown. The least stable, rather than average-sized grains move when instantaneously acted upon by the flowing fluid and, conversely, the most rapidly settling grains deposit. Grain stability is only partially dependent on particle size (weight in water). Our manipulative experiments clearly show that bed roughness and microbial adhesion influence τ_c and, to a lesser extent, bed roughness influences τ_d . Thus, the concept of a critical stress, if associated with a particle size, can only be applied unambiguously to individual grains or to grains of

equivalent size (our measurements). Even for grains of equivalent size, critical stresses vary about a central tendency (Fig.3).

Hjulstrom (1935) postulated that deposition would occur at two thirds of the critical erosion velocity for particles greater than 5 mm. Menard (1950) extended this prediction to finer sediments and due to Sundborg's (1956) review, it has gained wide acceptance today (e.g., Allen, 1965; Postma, 1967; Kennett, 1982, p.517). While we have presented all our results in the more consistent terms of critical stresses, we can reformulate our results in terms of critical mean velocities to allow them to be plotted on a Hjulstrom curve. Our results differ dramatically (Fig.10) from Hjulstrom's extrapolation. Our estimates of the ratio of τ_d to τ_e under abiotic conditions suggest that it varies from about 1 for coarse silt to 1/6 for fine silt (Figs.2 and 4), compared to 10^{-2} - 10^{-3} (Hjulstrom, 1935) and $\frac{3}{4}$ - $\frac{1}{4}$ (Allen, 1965). For natural sediments, ubiquitously covered with microbes, the results of our manipulative experiments suggest that variations in τ_e will influence the magnitude of the ratio much more than will variations in τ_d since τ_e can increase substantially due to microbial adhe-

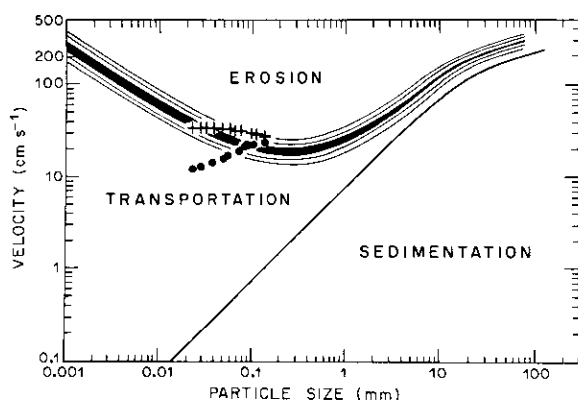


Fig.10. Original Hjulstrom plot separating regions of erosion, deposition and transportation, with our data superimposed. Dots represent critical particle deposition velocities, and crosses represent critical particle erosion velocities. Velocities for our points are calculated for a height of 100 cm above the bed (u_{100}) from the formula $u_{100}/u_* = 2.5 \ln(100u_*/\nu) + 4.9$, where u_* is shear velocity (cm s^{-1}) and ν is kinematic viscosity ($\text{cm}^2 \text{s}^{-1}$) (cf. Middleton and Southard, 1984).

sion. Thus, the demarcation between erosion, transport and sedimentation is not distinct. By increasing or decreasing the local boundary shear stress by $6 \times$ for fine silt, for example, biogenous structures and activities (e.g., tubes, pits and feeding appendages) can shift the transport condition from erosion to deposition or vice versa.

Acknowledgements

This work was supported by the Office of Naval Research contract N00014-87-K-0160; it carries University of Washington, School of Oceanography contribution number 1794. We thank P. Yager, D. Penry, P. Hill, B. Dade and R. Wheatcroft for surgery on earlier drafts and the Director of Friday Harbor Laboratories for use of excellent facilities.

References

- Allen, J.R.L., 1965. A review of the origin and characteristics of recent alluvial sediments. *Sedimentology*, 5: 89-191.
- Bagnold, R.A., 1956. The flow of cohesionless grains in fluids. *Philos. Trans. R. Soc. London, Ser. A*, 249: 235-297.
- Bennett, M.K. and Zisman, W.A., 1968. Effect of adsorbed water on the critical surface tension of wetting on metal surfaces. *J. Colloid Interface Sci.*, 28: 243-249.
- Bennett, M.K. and Zisman, W.A., 1969. Effect of adsorbed water on wetting properties of borosilicate glass, quartz and sapphire. *J. Colloid Interface Sci.*, 29: 413-423.
- Bowen, B.D., 1978. Fine particle deposition in smooth channels. Ph.D. Dissert., Univ. British Columbia, Vancouver, 439 pp.
- Bowen, B.D. and Epstein, N., 1979. Fine particle deposition in smooth parallel plate channels. *J. Colloid Interface Sci.*, 72: 81-97.
- Box, G.E.P., Hunter, W.G. and Hunter, J.S., 1978. *Statistics for Experimenters*. Wiley, New York, 653 pp.
- Butman, C.A., 1987. Larval settlement of soft-sediment invertebrates: the spatial scales of pattern explained by active habitat selection and the emerging role of hydrodynamical processes. *Oceanogr. Mar. Biol. Annu. Rev.*, 25: 113-165.
- Davis, R.H. and Acrivos, A., 1985. Sedimentation of noncolloidal particles at low Reynolds numbers. *Annu. Rev. Fluid Mech.*, 17: 91-118.
- Derjaguin, B.V. and Landau, L., 1941. Theory of the stability of strongly charged lyophobic sols and of the adhesion of strongly charged particles of electrolytes. *Acta Phys-Chim. U.R.S.S.*, 14: 633-662.

- Einstein, H.A. and Krone, R.B., 1962. Experiments to determine modes of cohesive sediment transport in salt water. *J. Geophys. Res.*, 67: 1451-1462.
- Fowler, H.W. and McKay, A.J., 1980. The measurement of microbial adhesion. In: R.C.W. Berkely, J.M. Lynch, J. Melling, P.R. Rutter and B. Vincent (Editors), *Microbial Adhesion to Surfaces*. Ellis Horwood, West Sussex, England, pp.143-161.
- Gardner, W.D. and Southard, J.B., 1975. Dynamics of boundary-layer deposition: A flume investigation. *Trans. Am. Geophys. Union*, 56: 372 (Abstr).
- Goldman, A.J., Cox, R.G. and Brenner, H., 1967. Slow viscous motion of a sphere parallel to a plane wall — II Couette flow. *Chem. Eng. Sci.*, 22: 653-660.
- Graf, W.H., 1971. *Hydraulics of Sediment Transport*. McGraw-Hill, New York, 513 pp.
- Grant, W.D., Boyer, L.F. and Sanford, L.P., 1982. The effects of bioturbation on the initiation of motion of intertidal sands. *J. Mar. Res.*, 40: 659-677.
- Heezen, B.C. and Hollister, C., 1964. Deep-sea current evidence from abyssal sediments. *Mar. Geol.*, 1: 141-174.
- Hjulstrom, F., 1935. Studies of the morphological activity of rivers as illustrated by the River Fyris. *Bull. Mineral. Geol. Inst. Univ. Upps.* 25: 221-528.
- Hollander, M. and Wolfe, D.A., 1973. *Nonparametric Statistical Methods*. Wiley, New York, 503 pp.
- Hubbe, M.A., 1981. Adhesion and detachment of biological cells *in vitro*. In: S.G. Davison and W.K. Liu (Editors). *Prog. Surf. Sci.*, 11: 65-138.
- Hunt, J.R., 1986. Particle aggregate breakup by fluid shear. In: A.J. Mehta (Editor), *Lecture Notes on Coastal and Estuarine Studies*. (Estuarine Cohesive Sediment Dynamics, 14.) Springer, New York, pp.85-109.
- Hunter, K.A. and Liss, P.S., 1979. The surface charge of suspended particles in estuaries and coastal waters. *Nature*, 282: 823-825.
- Kamphuis, J.W. and Hall, K.R., 1983. Cohesive material erosion by unidirectional current. *J. Hydraul. Eng.*, 109: 49-61.
- Kennett, J.P., 1982. *Marine Geology*. Prentice-Hall, Englewood Cliffs, N.J., 813 pp.
- Lavelle, J.W. and Mofjeld, H.O., 1987. Do critical stresses for incipient motion and erosion really exist? *J. Hydraul. Eng.*, 113: 370-385.
- Loeb, G.I., 1985. The properties of nonbiological surfaces and their characterization. In: D.C. Savage and M. Fletcher (Editors), *Bacterial Adhesion*. Plenum, New York, pp.111-128.
- Loeb, G.I. and Niehof, R.A., 1975. Marine conditioning films. In: R.E. Baier (Editor), *Applied Chemistry at Protein Interfaces*. Am. Chem. Soc., Washington, D.C., pp.319-335.
- Mantz, P.A., 1977a. Incipient transport of fine grains and flakes by fluids-extended Shields diagram. *Am. Soc. Civ. Eng., J. Hydraul. Div.*, 103: 601-615.
- Mantz, P.A., 1977b. Packing and angle of repose of naturally sedimented fine silica solids immersed in natural aqueous electrolytes. *Sedimentology*, 24: 810-832.
- Mantz, P.A., 1980. Laboratory flume experiments on the transport of cohesionless silicon silts by water streams. *Proc. Inst. Civ. Eng.*, 69: 977-994.
- Matthews, R.K., 1984. *Dynamic Stratigraphy: An Introduction to Sedimentation and Stratigraphy*. Prentice-Hall, Englewood Cliffs, N.J., 489 pp.
- McCave, I.N. and Swift, D.J.P., 1976. A physical model for the rate of deposition of fine-grained sediments in the deep sea. *Bull. Geol. Soc. Am.*, 87: 541-546.
- Mehta, A.J. and Partheniades, E., 1982. Resuspension of deposited cohesive sediment beds. In: B.L. Edge (Editor), *Proc. Coastal Eng. Conf., 18th. Am. Soc. Civ. Eng.*, Vol.2, pp.1569-1588.
- Menard, H.W., 1949. Transportation of bed-load by running water. Ph.D. Dissert., Arch. Harvard Univ., Harvard Coll. Libr., Cambridge, Mass., 82 pp.
- Menard, H.W., 1950. Sediment movement in relation to current velocity. *J. Sediment. Petrol.*, 20: 148-160.
- Middleton, G.V. and Southard, J.B., 1984. *Mechanics of Sediment Movement*. Soc. Econ. Paleontol. Mineral., Tulsa, Okla., 2nd Ed., 401 pp.
- Miller, D.C., Jumars, P.A. and Nowell, A.R.M., 1984. Effects of sediment transport on deposit feeding: scaling arguments. *Limnol. Oceanogr.*, 29: 1202-1217.
- Millero, F.J., 1974. Seawater as a multicomponent electrolyte solution. In: E.D. Goldberg (Editor), *The Sea*. Wiley, New York, pp.3-80.
- Moller, P.S., 1963. Radial flow without swirl between parallel discs. *Aeronaut. Q.*, 14: 163-186.
- Montague, C.L., 1986. Influence of biota on erodibility of sediments. In: A.J. Mehta (Editor), *Lecture Notes on Coastal and Estuarine Studies*. (Estuarine Cohesive Sediment Dynamics, 14.) Springer, New York, pp.251-269.
- O'Neill, M.E., 1968. A sphere in contact with a plane wall in a slow linear shear flow. *Chem. Eng. Sci.*, 23: 1293-1298.
- Overbeek, J.T.G., 1982. Strong and weak points in the interpretation of colloid stability. *Adv. Colloid Interface Sci.*, 16: 17-30.
- Owen, W.W., 1977. Problems in the modeling of transport, erosion and deposition of cohesive sediments. In: E.D. Goldberg, I.N. McCave, J.J. O'Brien and J.M. Steele (Editors), *The Sea*. Wiley, New York, Vol.6, pp.515-537.
- Parchure, T.M., 1984. Erosional behavior of deposited cohesive sediments. Ph.D. Dissert., Univ. Florida, Gainesville.
- Parchure, T.M. and Mehta, A.J., 1985. Erosion of soft cohesive sediment deposits. *J. Hydraul. Eng.*, 111: 1308-1326.
- Parsons, T.R., Maita, Y. and Lalli, C.M., 1984. *A Manual of Chemical and Biological Methods for Seawater Analysis*. Pergamon, New York, 173 pp.
- Partheniades, E., 1977. Unified view of wash load and bed material load. *Am. Soc. Civ. Eng., J. Hydraul. Div.*, 103(HY9): 1037-1057.
- Partheniades, E., 1984a. Two-dimensional model of mud transport. *Discussion. J. Hydraul. Eng.*, 110: 364-366.
- Partheniades, E., 1984b. Cohesive material erosion by unidirectional current. *Discussion, J. Hydraul. Eng.*, 110: 368-370.

- Pettijohn, F.J., 1975. *Sedimentary Rocks*. Harper and Row, New York, 628 pp.
- Postma, H., 1967. Sediment transport and sedimentation in the estuarine environment. In: G.H. Lauff (Editor), *Estuaries*. Am. Assoc. Adv. Sci., 83: 158-179.
- Raudkivi, A.J., 1976. *Loose Boundary Hydraulics*. Pergamon, New York, 397 pp.
- Rees, A.I., 1966. Some flume experiments with a fine silt. *Sedimentology*, 6: 209-240.
- Reineck, H.E. and Singh, I.B., 1980. *Depositional Sedimentary Environments*. Springer, New York, 549 pp.
- Ritter, D.F., 1978. *Process Geomorphology*. Brown, New York, 603 pp.
- Rubey, W.W., 1933. Settling velocities of gravel, sand and silt particles. *Am. J. Sci.*, 25: 325-338.
- Schaffernak, F., 1922. *Neue Grundlagen für die Berechnung der Geschiebeführung in Flussläufen*. Franz Deuticke, Leipzig und Wien.
- Schowalter, W.R., 1984. Stability and coagulation of colloids in shear fields. *Annu. Rev. Fluid Mech.*, 16: 245-261.
- Shafrin, E.G. and Zisman, W.A., 1967. Effect of adsorbed water on the spreading of organic liquids on soda-lime glass. *J. Am. Ceram. Soc.*, 50: 478-484.
- Shields, A., 1936. Application of the theory of similarity and turbulence research to the bedload movement. *Mitt. Preuss. Versl. Wasser Schiff*, 26.
- Smith, J.D., 1977. Modeling of sediment transport on continental shelves. In: E.D. Goldberg, I.N. McCave, J.J. O'Brien and J.M. Steele (Editors), *The Sea*. Wiley, New York, Vol.6, pp.539-577.
- Sokal, R.R. and Rohlf, F.J., 1969. *Biometry*. Freeman, San Francisco, Calif., 776 pp.
- Sundborg, A., 1956. The River Klaralven: a study in fluvial processes. *Geogr. Ann.*, 38: 125-316.
- Sundborg, A., 1967. Some aspects of fluvial sediments and fluvial morphology, 1. General views and graphic methods. *Geogr. Ann.*, 49: 333-343.
- Tate, M.W. and Clelland, R.C., 1957. *Nonparametric and Shortcut Statistics*. Interstate Print. Publ., Danville, Ill., 171 pp.
- Tritton, D.J., 1977. *Physical Fluid Dynamics*. Van Nostrand Reinhold, Workingham, Great Britain, 362 pp.
- Van Olphen, H., 1966. *An Introduction to Clay Colloid Chemistry*. Wiley, New York.
- Verwey, E.J.W. and Overbeek, J.T.G., 1948. *Theory of the Stability of Lyophobic Colloids*. Elsevier, Amsterdam.
- Westrich, J.T. and Berner, R.A., 1984. The role of sedimentary organic matter in bacterial sulfate reduction: the G model tested. *Limnol. Oceanogr.* 29: 236-249.
- White, J.S., 1970. Plane bed thresholds of fine grained sediments. *Nature*, 228: 152-153.
- Wiberg, P.L. and Smith, J.D., 1985. A theoretical model for saltating grains in water. *J. Geophys. Res.* 90(4): 7341-7354.

•
•
•

•
•
•